A Generalized Model for 3D Compton Scatter in Single Photon Emission Computed Tomography Using Slice-by-Slice Blurring and Scatter Projection Rebinning

Chuanyong Bai[1], Gengsheng L. Zeng[2], Grant T. Gullberg[2]
[1]ADAC Laboratories, 540 Alder Drive, Milpitas, CA95035
[2]MIRL/CAMT, 729 Arapeen Drive, SLC, UT84108

Abstract

The modeling of 3D Compton scatter in SPECT is complicated by the use of a variety of collimator geometry. To date, effective and efficient modeling of 3D Compton scatter in parallel-beam SPECT has been made possible by Frey and Tsui [1], Zeng et al [2], and Bai et al [3]. For fan-beam and cone-beam SPECT, the model in [3] can effectively model first order 3D Compton scatter. But for varying-focal-length fan-beam and cone-beam SPECT, no effective scatter models have been developed so far.

We propose in this work a generalized model for 3D first order Compton scatter in SPECT for different collimator geometry. The slice-by-slice blurring technique in [3] is used to generate a complete set of first order Compton scatter projections; the scatter projections are then properly rebinned according to the specific collimator geometry to obtain the scatter estimation. When generating the complete set of scatter projections, a set of virtual planar detectors with parallel-beam collimation are used to orbit around the object for scatter detection. Detailed discussion of this generalized model is provided in the METHODS section.

I. INTRODUCTION

In SPECT data acquisition, Compton scattered events are detected inevitably along with the primary (non-scattered) events due to the finite energy resolution and finite spatial resolution of the detectors. A photon usually loses part of its energy and changes its direction after being Compton scattered. Improper handling of the scattered photons can thus lead to the incorrect positioning of the source photons, and as a consequence, the reconstructed images can be degraded both quantitatively and qualitatively.

The primary difficulty for Compton scatter compensation in SPECT imaging is to obtain accurate scatter estimation. There are two major categories of techniques to obtain scatter estimation. One is the direct scatter estimation from data acquired using scatter energy window(s). Techniques in this category are easy to implement but not accurate. The other one is the modeling of the scatter from the attenuation map and the emission map during image reconstruction. Techniques in this category can be accurate but are difficult to implement, especially when complicate collimator geometry is used.

There are many techniques developed for the modeling of Compton scatter in SPECT. 1) Using Monte Carlo simulation for each specific scan [4-6]. 2) Using physical measurement to obtain the scatter response of a specific scan setup, the measured response is used as a characteristic of the given SPECT system [7]. 3) Using ideal integration based on the scatter cross-section described by the Klein-Nishina formula [8-9]. 4) Using ray driven projector/backprojector to model first order Compton scatter [10-12]. 5) Using a slab derived scatter model [13-18]. 6) Using an effective scatter source estimation model [1,19]. And 7) using a slice-by-slice blurring technique to model 3D first order Compton scatter [2-3, 21]. While almost all these techniques are effective to model scatter for parallel-beam SPECT, only [3] and [20] have shown to be effective and efficient for fixed-focal-length fan-beam and [3] for fixed-focal-length cone-beam SPECT.

In this work, we develop a generalized model for 3D first order Compton scatter in SPECT, using the slice-by-slice blurring technique [3] and scatter projection rebinning technique. The application of this model in SPECT with slant-hole collimator, annular collimator, and fan-beam and cone-beam collimators with both fixed-focal-length and varying-focal-length are discussed.

II. METHODS

A. The slice-by-slice blurring technique for first order Compton scatter

There are three basic principles for the slice-by-slice blurring model for first order Compton scatter described in [3]. (1) For each projection angle, photons emitted from a point source and scattered at a scattering point can only be detected at a certain position at the detector surface due to the assumption of perfect collimation. This means that when the position of point source is given, there is a one-to-one relationship between the positions of the scattering point and the detecting point, and thus the scattering angle for the detected scattered photons is unique for each scattering point. Figure 1 shows an example in fan-beam geometry. (2) For a given point source, on a scattering slice which is parallel to the detector surface, the photon energy and scattering angle dependent factor of the scatter probability (given by the Klein-Nishina formula) has a 2D distribution. This 2D distribution can be approximated using a 2D Gaussian function, considering the energy detection probability, the energy of the incident photon, and the detection energy window. (3) The 2D Gaussian function of the scattering slice which is closer to the detector surface (and thus further from the point source) can be obtained by a slice-by-slice blurring from the 2D Gaussian function of a scattering slice which is further away from the detector surface.

The generation of scatter estimation using this technique includes three steps. Step 1: the generation of the intermediate scatter source image (ISSI) from the attenuation map using

slice-by-slice blurring. The value of each element of ISSI is the production of the source intensity, the effective attenuation from the point source to the scattering voxel, and the scattering angle dependent factor of the scatter probability at the scattering voxel. The solid angle subtended by the element with the origin at the point source is also considered. Step 2: the generation of the effective scatter source image (ESSI) from ISSI, which is a voxel-by-voxel multiplication operation of the ISSI and the linear attenuation coefficient map. And step 3: the projection of the ESSI using a slab-by-slab blurring model to generate the final scatter estimation [21].

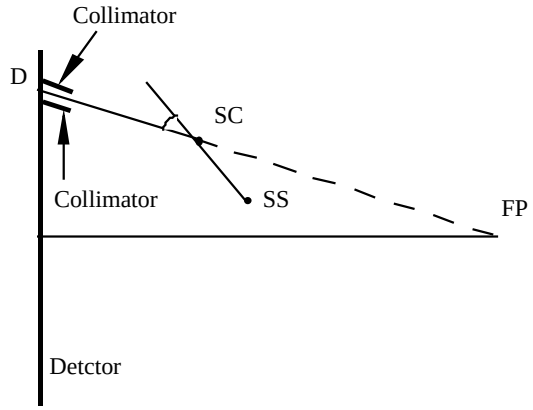

Figure 1. Photons that are originated from source SS and scattered at scattering point SC can only be detected at point D on the detector surface under the assumption of perfect collimation.

The slice-by-slice blurring model includes the non-uniform attenuation from the source to scattering point in Step 1 and from the scattering point to the detecting point in Step 3. The geometric point response effect of the SPECT system can also be included in Step 3. In Step 2, the effective non-uniform scatter probability of a scattering voxel is considered. Using this model, one can accurately estimate 3D first order Compton scatter along a give direction for any scattering media.

B. A generalized model for 3D Compton scatter

When photons shine on a scattering voxel, they can be scattered to a 4• solid angle, theoretically. We can divide this 4• solid angle to a series of sub-solid angles. The scattered photons in each sub-solid angle can then be detected by using a planar detector with parallel beam collimation. In this way, we can obtain a complete detection of the photons that are scattered by the scattering voxel. Figure 2 illustrates the basic idea of generating a complete set of scatter projections.

The generalized model includes the following two steps. **Step 1.** Using the slice-by-slice blurring model to generate a set of scatter projections, assuming that we use a set of virtual planar detectors with parallel collimation to detect the scattered photons. Each parallel scatter projection contains the scatter estimation for the corresponding sub-solid angle, and thus the set of parallel scatter projections form a complete scatter estimation. **Step 2.** For a given SPECT geometry, using an appropriate rebinning process to obtain the scatter estimation for all the detector bins. In this step, the set of generated scatter projections in Step 1 is used for rebinning.

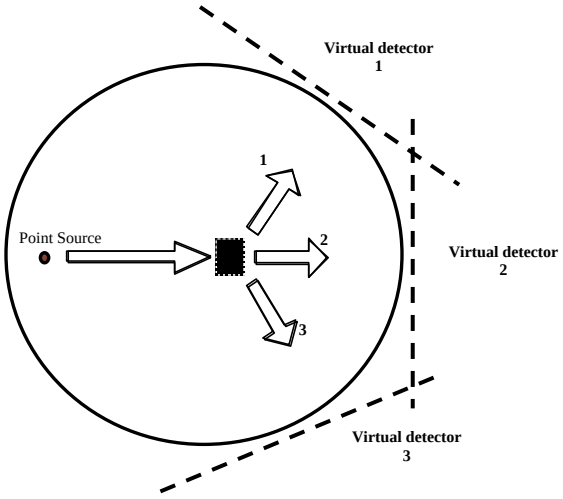

Figure 2. A complete scatter estimation can be obtained through slice-by-slice blurring model, using one virtual planar detector with parallel collimation at each sub-solid angle.

C. Implementation of the model

1. Slant hole collimation, planar detectors

For planar detectors with slant hole collimation [22], the collimation in each segment is essentially parallel. Figure 3 shows the geometry of a bilateral slant-hole collimator. The collimation directions of different segments are different. For each segment, one only needs to generate a series of parallel projections, which have different distances in the direction of the collimation, using virtual planar detectors (dashed lines in Figure 3) with parallel collimation. For a detector bin *i* on the slant detector, the rebinning procedure is to first determine its interception position (***k***, i) with one of the parallel scatter projections ***k*** , and then estimate its scatter using the scatter values of the bins closest to (***k***, i) of projection ***k***. If we use $bin\_size \cdot \cos(\beta)$ as the bin size in the slant direction, and *bin_size* in the parallel direction, no interpolation is needed for the rebinning. Here *bin_size* is the slant-hole collimator bin size and β is the slant angle. For this special collimation geometry, one can incorporate the asymetric geometric point response of the detector in Step 3 of the slice-by-slice blurring model during the generation of complete scatter estimation.

2. Parallel collimation, annular detectors

Figure 4 shows the geometry (transaxial cross section) of a SPECT system with annular detector and parallel collimation. In the axial direction of the detector, the collimation is also parallel. A complete set of scatter projection can be obtained by using a set of virtual parallel detectors evenly distibuted along the annular ring. For a detector bin corresponding to angle C in Figure 3, an accurate way to estimate its scatter is to generate a virtual parallel scatter projection (with same bin size as the annular detector) for this angle and pick up the scatter value directly. If only the

parallel projection in the neighboring angles A and B are generated for the sake of decreasing computational burden, an interpolation step should be taken for the rebinning. Explicitly, we first find the bins (A, i) and (B, j) on the planar parallel detectors at angles A and B that correspond to the detector bin in direction C. If their values are S(A, i) and S(B, j), then the scatter at the detector bin in angle C can be expressed as:

$$[S(A,\ i)\cdot(B-C)+S(B,\ j)\cdot(C-A)]/(B-A). \qquad (1)$$

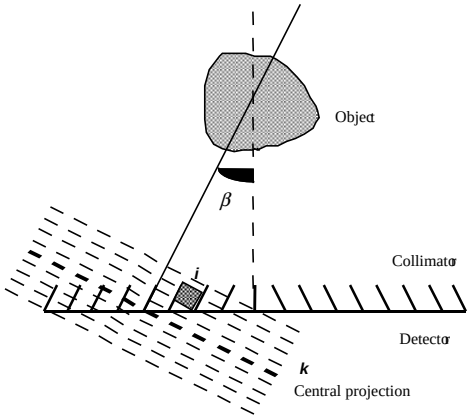

Figure 3. Bilateral slant-hole parallel collimation.

Note that here we simply consider the angular interpolations between neighboring projections. To be more accurate, a small compensation of solid angle difference should be made due to the longer distances from (A, i), and (B, j) to the center of rotation than the detector bin at angle C. One can project the bin to parallel projections A and B and then sum up the values of the projected bins. Thus equation (1) becomes:

$$\left[\sum_{i} S(A,i)\cdot(B-C)+\sum_{j} S(B,j)\cdot(C-A)\right]/(B-A) \qquad (2)$$

3. Fixed-focal-length fan-beam and cone-beam collimation, plane detectors

Figure 5 illustrates the geometry of a SPECT system with fixed-focal-length fan-beam collimation in the fan direction and parallel collimation in parallel direction. For each angle from the focal point to a detection bin in the fan direction, we generate a scatter projection using a virtual planar detector (dashed lines in Figure 5) with parallel collimation. The rebinning step assigns to the detector bin the scatter value of the central bin of the virtual parallel scatter projection. If one uses less number of angles than the number of bins to generate the scatter responses, the scattered value at each detector bin can be obtained with a simple angular interpolation as is the same as described in equation (1). However, when compensating for the changed solid angle, equation (2) should be slightly modified to reflect the fact that the projected bin(s) on one of the neighboring virtual projection are closer to the center of rotation, and thus the subtended angles are increased.

When performing SPECT scans using fixed-focal-length fan beam SPECT systems, sometimes a non-circular orbit is used [23] to avoid truncation or to make the line of focus remain fixed to the center of the organ of interest, etc. For these scans, the focal-point orbit function should be used to determine the relative position of the center of object matrix to the focal point and the detector surface at different projection angle for proper scatter projection rebinning and solid angle compensation.

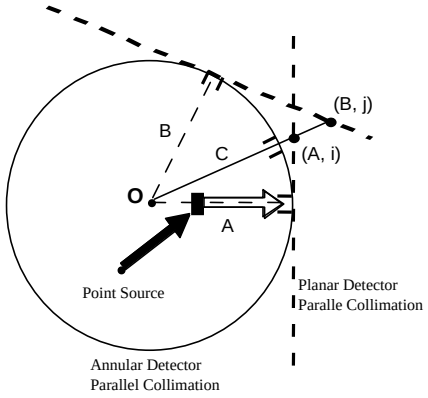

Figure 4. An annular detector with parallel collimation.

For planar detector with fixed-focal-length collimation, the generation of the complete set of scatter projection is three-dimensional. The scatter projection rebinning is also three-dimensional.

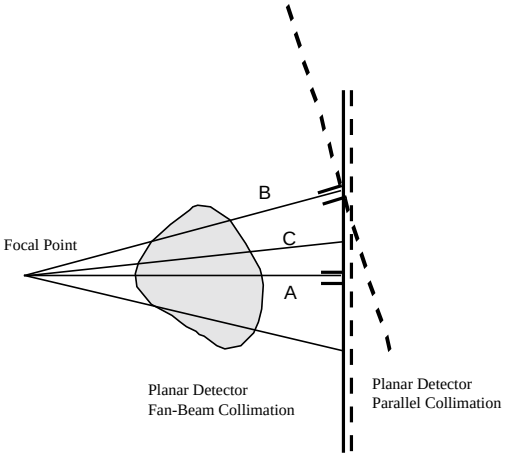

Figure 5. Fixed-focal-length fan-beam geometry.

4. Varying-focal-length fan beam and cone beam collimation, planar detectors

For varying-focal-length fan beam collimation and planar detectors, one can use the same scheme as for fixed-focal-length fan beam collimation and planar detectors to obtain the scatter estimation. The difference is that when rebinning, one should use the focal-length function [24, 25] to determine which parallel projections should be used for rebinning. The direction of these scatter projections are determined by the

detector bins and the position of the focal points corresponding to these bins.

For varying-focal-length cone-beam collimation, the generation of complete set of scatter projections should be three-dimensional, and the interpolation described in equation (2) should also be three-dimensional.

It should be noted that for SPECT imaging using varying focal-length fan-beam or cone-beam collimation and planar detector, the focal point closest to the detector surface should be out of the object of interest to avoid multiple images. However, this restriction is not needed for scatter estimation using this generalized scatter model.

III. DISCUSSION

The scatter model proposed in this work is based on the assumption that a complete first order 3D Compton scatter projection can be obtained by using a set of virtual planar detectors with parallel collimation. This assumption is accurate when enough number of parallel scatter projections are generated. Simulation studies for fixed-focal-length fan beam SPECT will be presented. Simulation studies for varying-focal-length fan-beam and cone-beam collimation will be performed when a proper simulator is available.

IV. REFERENCES

[1] Frey EC and Tsui BMW 1996 A new method for modeling the spatially-variant, object-dependent scatter response function in SPECT Record 1996 *IEEE Nucl. Sci. Symp. Med. Imag. Conf.* 1082-1086

[2] Zeng GL, Bai C, and Gullberg GT 1999 A projector/ backprojector with slice-to-slice blurring for efficient 3D scatter modeling *IEEE Trans. Med. Img.* **18** 722-273

[3] Bai C, Zeng GL, and Gullberg GT 2000 A slice-by-slice blurring model and kernel evaluation using the Klein-Nishina formula for 3D scatter compensation in parallel and converging beam SPECT *Phys. Med. Biol.* **45** 1275-1307

[4] Floyd CE, Jaszczak RJ, and Coleman RE 1989 Inverse Monte Carlo: A unified reconstruction algorithm *IEEE Trans. Nucl. Sci.* **36** 779-785

[5] Frey EC and Tsui BMW 1990 Parameterization of the scatter response function in SPECT imaging using Monte Carlo simulation *IEEE Trans. Nucl. Sci.* **37** 1308-1315

[6] Bowsher JE and Floyd CE, Jr. 1991 Treatment of Compton scatter in maximum-likelihood, expectation-maximization reconstruction of SPECT images *J. Nucl. Med.* **32** 1285-1291

[7] Beekman FJ, Frey EC, Kamphuis C, Tsui BMW, and Viergever MA 1994 A new phantom for fast determination of scatter response of a Gamma camera *IEEE Trans. Nucl. Sci.* **41** 1481-1488

[8] Cao ZJ, Frey EC, and Tsui BMW 1994 A scatter model for parallel and converging beam SPECT based on the Klein-Nishina formula *IEEE Trans. Nucl. Sci*. **41** 1594-1600

[9] Wells RG, Celler A, and Harrop R 1998 Analytical calculation of photon distributions in SPECT projections *IEEE Trans. Nucl. Sci.* **45** 3202-3214

[10] Welch A, Gullberg GT, Christian PE, and Datz FL 1995 A transmission-map-based scatter correction technique for SPECT in inhomogeneous media *Med. Phys.* **22** 1627-1635

[11] Welch A and Gullberg GT 1997 Implementation of a model-based non-uniform Scatter correction scheme for SPECT *IEEE Trans. Med. Imag.* **16** 717-726

[12] Laurette I, Welch A, Christian PE, and Gullberg GT A three-dimensional transmission-map-based scatter correction technique for SPECT in inhomogeneous media (submitted to) *Phys. Med. Biol*.

[13] Frey EC, Ju ZW, and Tsui BMW 1993 A fast projector-backprojector pair modeling the asymmetric, spatially varying scatter response function for scatter compensation in SPECT imaging *IEEE Trans. Nucl. Sci.* **40** 1192-1197

[14] Frey EC and Tsui BMW 1993 A practical method for incorporating scatter in a projector-backprojector for accurate scatter compensation in SPECT *IEEE Trans. Nucl. Sci*. **40** 1107-1116

[15] Beekman FJ, Eijkman EGJ, Viergever MA, Borm GF, and Slijpen ETP 1993 Object Shape dependent PSF model for SPECT imaging *IEEE Trans. Nucl. Sci.* **40** 31-39

[16] Beekman FJ and Viergever MA 1995 Fast SPECT simulation including object Shape dependent scatter *IEEE Trans. Med. Imag*. **14** 271-282

[17] Beekman FJ, Kamphuis C, and Viergever MA 1996 Improved SPECT quantitation Using fully three-dimensional iterative spatially variant scatter response compensation *IEEE Trans. Med. Img*. **15** 491-499

[18] Beekman FJ, Kamphuis C, and Frey EC 1997 Scatter compensation methods in 3D iterative SPECT reconstruction: A simulation study *Phys. Med. Biol.* **42** 1619-1632

[19] Kadrmas DJ, Frey EC, Karimi SS, and Tsui BMW 1998 Fast implementation of reconstruction-based scatter compensation in fully 3D SPECT image reconstruction *Phys. Med. Biol*. **43** 857-873

[20] Bai C, Zeng GL, and Gullberg GT 1998b A fan-beam slice-by-slice blurring model for scatter, geometric point response, and attenuation corrections in SPECT using the iterative OS-EM algorithm (abstract) *J. Nucl. Med*. **39** 120P

[21] Bai C, Zeng GL, Gullberg GT, DiFilippo F, and Miller S 1998a Slab-by-slab Blurring model for geometric point response correction and attenuation correction using iterative reconstruction algorithm *IEEE Trans. Nucl. Sci.* **45** 2168-2173

[22] Clack R, Christian PE, Defrise M, and Welch AE 1996 Image reconstruction for a novel SPECT system with rotating slant-hole collimators Conf. Rec. 1995 *IEEE Med. Imag. Conf.* 1948-1952

[23] Gullberg GT and Zeng GL 1995 Backprojection filtering for variable orbit fan-beam tomography *IEEE Trans. Nucl. Sci.* **42** 1257-1266

[24] Zeng GL and Gullberg GT 1994 A backprojection filtering algorithm for a spatially varying focal length collimator *IEEE Trans. Med. Imag*. **13** 549-556

[25] Zeng GL, Gullberg GT 1998 Iterative and analytical reconstruction algorithms for varying-focal-length cone-beam projections *Phys. Med. Biol*. **43** 811-821